

Femtosecond strong-field coherent control of nonresonant ionization with shaped pulses

Qiu-Nan Tong(佟秋男), Zhen-Zhong Lian(廉振中), Liang Zhao(赵亮), Hong-Xia Qi(齐洪霞), Zhou Chen(陈洲), Zhan Hu(胡湛)

Citation: Chin. Phys. B . 2019, 28(3): 033201. **doi:** 10.1088/1674-1056/28/3/033201
Journal homepage: http://cpb.iphy.ac.cn; http://iopscience.iop.org/cpb

What follows is a list of articles you may be interested in

Angle-resolved spectra of the direct above-threshold ionization of diatomic molecule in IR+XUV laser fields

Shang Shi(石尚), Fa-Cheng Jin(金发成), Bing-Bing Wang(王兵兵)

Chin. Phys. B . 2019, 28(2): 023202. **doi:** 10.1088/1674-1056/28/2/023202

Validity of extracting photoionization time delay from the first moment of streaking spectrogram

Chang-Li Wei(魏长立), Xi Zhao(赵曦)

Chin. Phys. B . 2019, 28(1): 013201. **doi:** 10.1088/1674-1056/28/1/013201

Low-order harmonic generation of hydrogen molecular ion in laser field studied by the two-state model

Ling-Ling Du(杜玲玲), Guo-Li Wang(王国利), Peng-Cheng Li(李鹏程), Xiao-Xin Zhou(周效信)

Chin. Phys. B . 2018, 27(11): 113201. **doi:** 10.1088/1674-1056/27/11/113201

Field-free orientation of diatomic molecule via the linearly polarized resonant pulses

Li Su-Yu, Guo Fu-Ming, Wang Jun, Yang Yu-Jun, Jin Ming-Xing

Chin. Phys. B . 2015, 24(10): 104205. **doi:** 10.1088/1674-1056/24/10/104205

Ultrafast population transfer in a Λ-configuration level system driven by few-cycle laser pulses

Zhang Wen-Jing, Xie Xiao-Tao, Jin Lu-Ling, Bai Jin-Tao

Chin. Phys. B . 2013, 22(11): 114210. **doi:** 10.1088/1674-1056/22/11/114210

Femtosecond strong-field coherent control of nonresonant ionization with shaped pulses*

Qiu-Nan Tong(佟秋男)[1,2], Zhen-Zhong Lian(廉振中)[1,2], Liang Zhao(赵亮)[1,2], Hong-Xia Qi(齐洪霞)[1,2], Zhou Chen(陈洲)[1,2,†], and Zhan Hu(胡湛)[1,2,‡]

[1] *Institute of Atomic and Molecular Physics, Jilin University, Changchun* 130012, *China*

[2] *Advanced Light Field and Modern Medical Treatment Science and Technology Innovation Center of Jilin Province, Jilin University, Changchun* 130012, *China*

(Received 26 October 2018; revised manuscript received 14 January 2019; published online 26 February 2019)

The strong-field coherent control of the nonresonant ionization of nitrous oxide using shaped pulses is investigated. We study the dependence of periodic coherent oscillation of the total ionization yield on the variation of laser phase parameters. The physical mechanism of the strong-field coherent control is investigated experimentally and theoretically by the nonresonant spectral phase interferences in the frequency domain. We show that the intense shaped pulses with broadband and off-resonance can be used as a robust strong-field coherent control method.

Keywords: coherent control, nonresonant ionization, shaped pulse

PACS: 32.80.Rm, 42.50.Hz **DOI:** 10.1088/1674-1056/28/3/033201

1. Introduction

As a robust method, the coherent control scheme is used to steer a quantum system to the pre-defined target or dynamical behavior by the transfer of coherence properties from light to the quantum system. The coherent interference is one of the most basic and important theories in quantum mechanics, which can be used to control the quantum systems by constructive or destructive interference between initial state and final state. The development of various laser sources with pulse widths comparable to the time scale of quantum dynamics, i.e., the femtosecond regime, and the increasing capabilities of pulse shaping in amplitude, phase, and polarization have been demonstrated to be effective in manipulating both simple and complex systems such as atoms, molecules, and semiconductors.

There are two main control schemes classified by the intensity of laser interacting with model systems. When the applied laser field is weak, and the perturbation theory applies, there is a direct relationship between the laser spectral phases of different frequency components and the phases of the pathways to the final state. As outlined by Shapiro and Brumer,[1] the dynamic mechanisms in the perturbative regime are related to laser field (or higher order) spectral interferences.[2–5] For instance, two-photon transition processes such as resonant two-photon absorption (TPA) and nonresonant TPA can be selectively enhanced or suppressed.[2,6] However, when the applied electric fields are strong, it is equivalent to presenting an additional degree of freedom, and the perturbation theory is invalid. The level broadening and shift of the quantum systems make the spectral interference treatments rather complicated. The phases of the pathways between initial and final states are no longer directly related to that of the laser field. Siberberg and co-workers proposed a "simple route" to strong-field coherent control.[6] They showed that the real electric field with only one quadrature in the complex plane can be used to deal with the issue, which can symmetrically cancel the power broadening effects. Some strong-field experiments have been interpreted in terms of selective population of dressed states (SPODS), which establishes the general framework of strong-field control mechanisms such as photon locking (PL),[7] (stimulated) rapid adiabatic passage (RAP, STIRAP),[8] and their combinations. The control of SPODS has been accomplished using chirped pulses, pulse sequences, sinusoidal phase-modulated shaped pulses, and their combinations, where the theoretical methods involve the dressed states model,[9] Autler–Townes model,[10] and Bloch-vector model.[8] Another degree of freedom in coherent control is phase interferences caused by broadband laser pulse, which includes both resonant frequency and nonresonant frequency components. Amitay's group pointed out that the pulse-bandwidth dependence interferences can be attributed to the third-order perturbative interaction in the weak field regime.[11] Weinacht and co-workers systematically analyzed the behavior of interferences driven by wide bandwidth shaped pulses.[12] They proposed that the interferometric modulations, where resonant and nonresonant ones present simultaneously, are dominated by interference between resonant and nonresonant pathways rather than interference between the

*Project supported by the National Natural Science Foundation of China (Grant No. 11374124).

†Corresponding author. E-mail: phy_cz@jlu.edu.cn

‡Corresponding author. E-mail: huzhan@jlu.edu.cn

© 2019 Chinese Physical Society and IOP Publishing Ltd

different resonant pathways in the weak field regime, and the interference pattern is most easily understood by time-domain dynamics rather than nonperturbative theory in the strong field regime. Furthermore, some research work has demonstrated that the coherent control can be expanded from a few photons to many photons conditions.[13–15] In recent years, a new type of photoelectron wavepacket interferences in ionization processes was presented experimentally and theoretically. For the simplest case, the photoelectron angular distributions (PAD) can be modulated by the interference between different photoelectron angular momentum components yielded by ionization, and the control over the interferograms has been investigated in the energy-domain.[16,17] In the time-domain, the final measured interferograms result from the coherent superposition of all the ionization pathways which happens at any moment during the pulse, because the observed result is integrated over the entire pulse duration.[18,19] Unlike spectral phase interferences determined by the phase between different pathways, the interferences in ionization are due to the angle (and phase) interferences of photoelectron wavepackets using polarization multiplexing, such as dynamic dimensionality identification,[20] electron vortices,[21] photoelectron circular dichroism,[22] and molecular frame reconstruction[17] using polarization shaped pulses.

In the current paper, we show one type of coherent control over nonresonant ionization making use of nonperturbative control by sinusoidal phase modulated shaped pulses. Different from previous strong field coherent control research where spectral phase interferences based on perturbation theory are invalid, we study the dependence of the periodic coherent oscillation of the total ionization yield on the variation of the laser parameters, and propose that the coherent oscillation is caused by periodic interferences of the laser spectral phase. We argue that, to a certain extent, spectral phase interference still plays an important role in some coherent control experiments in the strong field region, such as the nonresonant ionization process using intense broadband laser field. In addition, the implementation of control can be realized not only by the interference effects on particular quantum excitation channels, but also the assembly effect caused by the interferences of many excitation channels. The nitrous oxide molecule is chosen as our model system. Nitrous oxide, also known as laughing gas, occupies a very small proportion of the earth's atmosphere. However, it has two orders of magnitude more global warming effect as a greenhouse gas than carbon dioxide. Nitrous oxide is also the main reason for ozone depletion because of the gradually increase of its emission. Due to these two aspects, the nitrous oxide molecule has attracted wide attention of many scientists in atmospheric science and environmental chemistry. Much work has been devoted to studies of the ionization and dissociation of nitrous oxide by positive ions, photons, electron impact, and negative-ion impact.

2. Experiment

2.1. Sinusoidal phase modulation

A common method to modulate a laser pulse is to use a 4-f optical setup.[23] The modulation by Sinusoidal phase function is operated in frequency domain, but the envelope in the time domain usually attracts people's attention as well. We analyze the envelope of time-frequency Fourier transform in this section, and show the important properties of the modulated pulses. We start with the unmodulated laser field with horizontal polarization[24]

$$E_{\rm in}(t) = \varepsilon_{\rm in}(t)\,{\rm e}^{{\rm i}\omega_0 t}, \tag{1}$$

where ω_0 is the carrier frequency and $\varepsilon_{\rm in}(t)$ denotes, in general, the electric field envelope. The sinusoidal phase functions loaded to two masks of the modulation device,

$$\varphi_1 = A_1 \sin[(\omega-\omega_{\rm ref})T_1+\phi_1], \tag{2}$$

$$\varphi_2 = A_2 \sin[(\omega-\omega_{\rm ref})T_2+\phi_2], \tag{3}$$

modulate the spectrum $E_{\rm in}(\omega)$ in frequency domain and the modulated field is give by

$$E_{\rm out}(\omega) = E_{\rm in}(\omega)\,{\rm e}^{{\rm i}(\varphi_1+\varphi_2)}, \tag{4}$$

where A defines the amplitude of the modulation function, T the frequency of the sinusoidal function oscillation, and ϕ the constant phase offset. The $\omega_{\rm ref}$ is introduced experimentally to describe the initial reference angular frequency of the sinusoidal phase function with respect to the central angular frequency of the laser spectrum.

First, we discuss a special case of $A = A_1 = A_2$, $T = T_1 = T_2$, and $\phi = \phi_1 = \phi_2$, resulting in a shaped pulse sequence with constant linear polarization. Equation (4) can be rewritten as

$$E_{\rm out}(\omega) = E_{\rm in}(\omega)\,{\rm e}^{2{\rm i}A\sin[(\omega-\omega_{\rm ref})T+\phi]}. \tag{5}$$

We can further obtain the modulated electric field in time domain by the Jacobi–Anger identity and time-frequency Fourier transform[25]

$$E_{\rm out}(t) \propto {\rm e}^{{\rm i}\omega_0 t}\sum_{n=-\infty}^{\infty} J_n(A)\varepsilon_{\rm in}(t+nT)\,{\rm e}^{{\rm i}n(\Delta\omega T+\phi)}, \tag{6}$$

where $\Delta\omega = \omega_0 - \omega_{\rm ref}$ denotes the difference between the laser carrier frequency and the reference frequency of the sinusoidal phase function, and J_n is the Bessel function of the first kind and order n. Therefore, the modulated electrical field envelope $\varepsilon_{\rm out}(t)$ can be written as

$$\varepsilon_{\rm out}(t) \propto \sum_{n=-\infty}^{\infty} J_n(A)\varepsilon_{\rm in}(t+nT)\,{\rm e}^{{\rm i}n(\Delta\omega T+\phi)}. \tag{7}$$

From Eq. (7), we can see that the sinusoidal phase modulation produces a laser pulse sequence in time domain with a same

sub-pulse temporal separation determined by the parameter T. The envelope of each sub-pulse is a replica of the unmodulated pulse envelope $\varepsilon_{\rm in}(t)$ with reduced intensity, and the difference of relative phases between adjacent sub-pulses is determined by $\Delta\omega T+\phi$.

Next, we discuss the case of $A=A_1=A_2$, $T=T_1=T_2$, and $\phi=\phi_1=-\phi_2$, resulting in a shaped pulse sequence with varying polarization. In addition, a quarter-wave plate (QWP) is placed at the exit of the pulse shaper, with the fast axis of the QWP along the horizontal direction. The same as the analysis above, the modulated electric field in time domain can be obtained as

$$\boldsymbol{E}_{\rm out}(t)\propto {\rm e}^{{\rm i}\omega_0 t}\varepsilon_{\rm out}(t). \tag{8}$$

The modulated electrical field envelope $\varepsilon_{\rm out}(t)$ can be written as

$$\varepsilon_{\rm out}(t)\propto \sum_{n=-\infty}^{\infty} J_n(A)\varepsilon_{\rm in}(t+nT)\,{\rm e}^{{\rm i}n(\Delta\omega T+\phi)}\boldsymbol{r}_n. \tag{9}$$

The temporal separation between sub-pulses is determined by the parameter T, and the envelope of each sub-pulse is a replica of the unmodulated pulse with reduced intensity. The difference of relative phases between adjacent sub-pulses is determined by $\Delta\omega T+\phi$. The $\boldsymbol{r}_n$ indicates the unit vector of the n-th sub-pulse polarization direction. The sub-pulse with $n=0$ is horizontally polarized light. But the n-th sub-pulse ($n\neq 0$) has an azimuthal angle of $n\phi$ with respect to the horizontal direction. For example, the angle of sub-pulse with $n=1$ is ϕ. In addition, we can find that the angle between adjacent sub-pulses is ϕ. Figure 1 shows schematically the laser fields using two modulation methods.

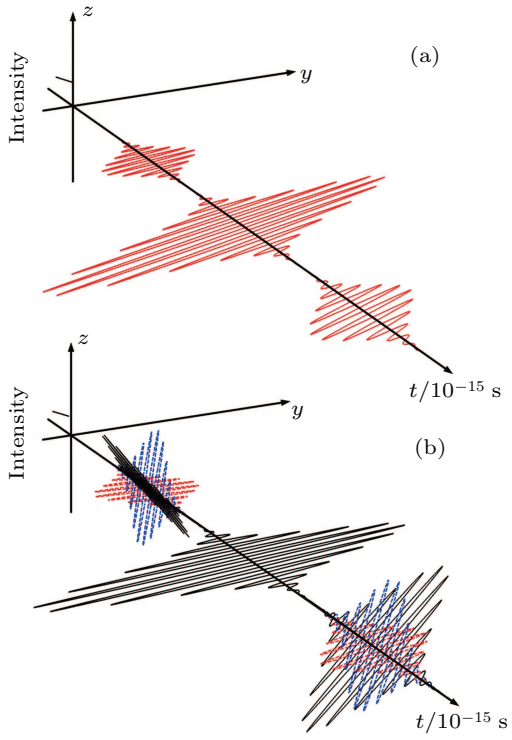


Fig. 1. Diagrams of the laser electric fields using two modulation methods for shaped pulse sequences with (a) constant (horizontal) polarization (red bold lines) and (b) varying polarization (black bold lines). In panel (b), the red dashed lines and blue dashed lines indicate the projections of the laser electric fields in horizontal and vertical directions, respectively.

2.2. Experimental setup

The femtosecond laser pulses are generated by an amplified laser system (Spectra-Physics, Solstice Ace, 1 kHz, 35 fs, 6 mJ) and modulated by the polarization pulse shaper setup, which is based on a design by Gerber *et al.*[26] A concave focusing mirror ($f=75$ mm) is used to focus the laser to obtain an intensity up to 4×10^{14} W/cm^2 at the focal point with 40 μJ/pulse. The total ionization yield and kinetic energy distribution of electrons are measured by a cold-target recoil-ion-momentum spectrometer (COTRIMS).[27] First, we measure the ionization yield and kinetic energy distribution of electrons using shaped pulse sequences with varying polarization, as functions of sinusoidal parameters T and ϕ. Then we investigate the effect of polarization changing on the ionization yield and kinetic energy distribution using a shaped pulse sequence with constant linear polarization. In all experiments, the value of A is fixed at 0.5, which can produce a three-pulse sequence. The parameter T ranges from 80 fs to 700 fs, and $-\pi$ to π for ϕ.

The precise generation of polarization-shaped femtosecond laser pulses with a well-designed polarization profile in time domain is challenging in the laboratory.[28] The multiphoton intrapulse interference phase scan (MIIPS) and polarization-labeled interference versus wavelength for only a glint (POLLIWOG) methods are used to ensure that the pulse without modulation is transform limited, and the polarization-shaped pulses are accurate.

3. Results and discussion

In this section, we present the experimental results obtained by the nonresonant ionization of nitrous oxide using intense ultrashort shaped pulse sequences with varying or constant polarization modulated by sinusoidal phase functions. Then we study the total ionization yield as functions of phase parameters. We also measure the kinetic energy distribution of the ionized electrons and try to investigate the mechanisms of coherent control of different ionization channels based on the nonresonant two-photon interference theory.

First, we study the ionization yield dependence on phase parameter using a shaped pulse sequence with varying polarization. The ionization yield distribution upon variation of the phase parameters T and ϕ is shown in Fig. 2 as a two-dimensional graph. The yield oscillates obviously with both T (pulse interval) and ϕ, in which the oscillation period with T is about 200 fs, and 2π with ϕ. But the regularity seems to

be broken when T is smaller than 100 fs. We believe this is due to the optical interference between sub-pulses when they overlap in time domain.[29] The peak intensity of the oscillation gradually reduces with increasing T, which means that the total ionization yield also shows a decreasing trend. By changing T and ϕ, one can control the total ionization yield using the shaped pulse sequence with varying polarization. For instance, figure 3(a) shows two horizontal slices of data from the two-dimensional ionization yield distribution in Fig. 2 at $\phi = 0$ and π. Both ionization yield curves oscillate with T, and the phase of the oscillation is shifted by π at $\phi = 0$ with respect to that at $\phi = \pi$. The π phase shift of the curves equals the difference between the two values of the parameter ϕ. Thus, the ϕ parameter can be used as a direct phase control method. Two vertical slices of data from the two-dimensional ionization yield distribution in Fig. 2 at $T = 338$ fs and $T = 435$ fs are shown in Fig. 3(b). The 2π oscillation period is caused by the inherent period when applying phase to the spatial light modulator. The difference between the two values of T is chosen to be about half of the T oscillation period in Fig. 2, which is in agreement with the π phase shift of the two oscillation curves. Thus, the T parameter can also be used as a reliable coherent control method. The modulation depth is significantly larger at $T = 338$ fs than that at $T = 435$ fs. This is because the parameter T not only modulates the phase of the laser pulse in Eq. (5), but also affects the shape of the laser pulse in time domain, as discussed in the experiment section. The modulation of the laser phase results in periodic oscillation. In the time domain, the modulation of the laser phase is mainly determined by the difference of relative phases between adjacent sub-pulses, i.e., $\Delta\omega T + \phi$. When T is fixed, the oscillation period of ϕ is 2π, which consists of the oscillation period of the ionization yield. When ϕ is fixed, the oscillation period of $\Delta\omega T$ is 2π. Therefore, 200 fs (the oscillation period of the ionization yield) is the value of T that makes $\Delta\omega T$ equal to 2π. However, the influence on the laser pulse, i.e., the increase of laser sub-pulse separation from 338 fs to 434 fs, probably leads to the difference in the modulation depth, because of stronger decoherence effect at longer time.

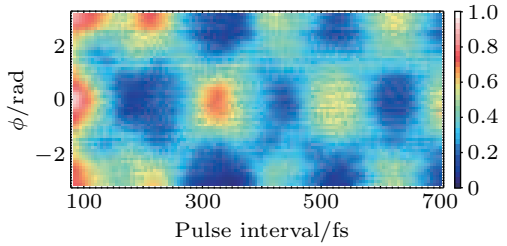


Fig. 2. The two-dimensional ionization yield distribution upon variation of the phase parameters T (pulse interval) from 80 fs to 800 fs and ϕ from $-\pi$ to π for fixed value of $A = 0.5$ using shaped pulse sequence with varying polarization.

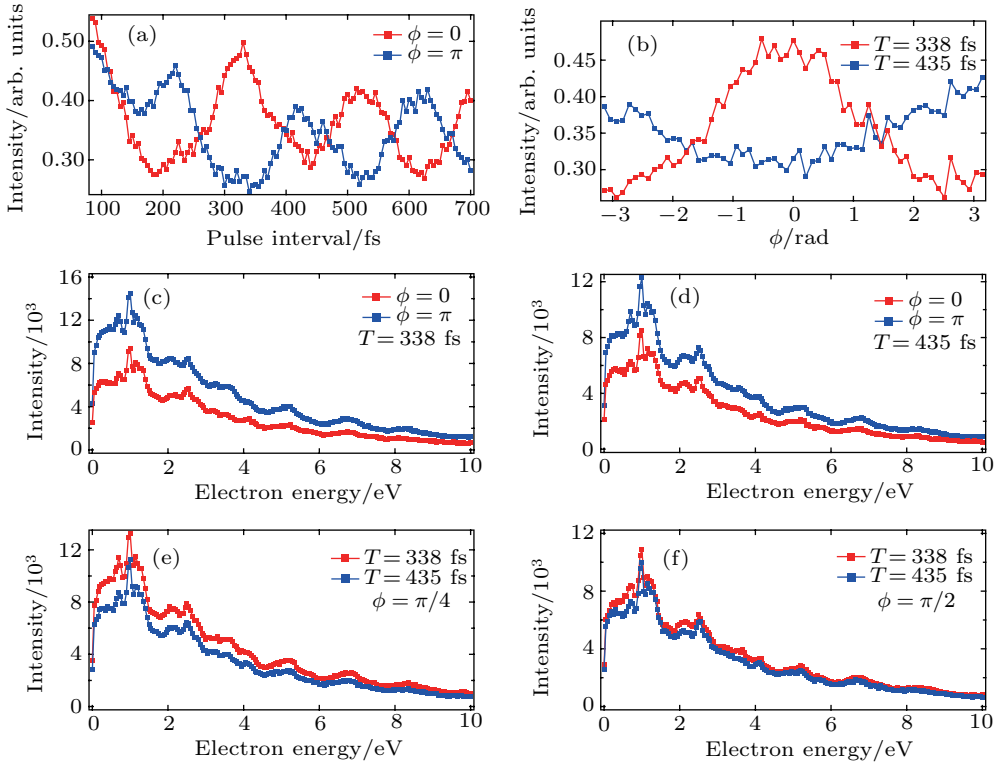


Fig. 3. (a) Horizontal slices of data from the two-dimensional ionization yield distribution in Fig. 2 at $\phi = 0$ (red) and π (blue). (b) Vertical slices of data from the two-dimensional ionization yield distribution in Fig. 2 at $T = 338$ fs (red) and $T = 435$ fs (blue). The photoelectron kinetic energy distribution curves with $\phi = 0$ (red) and $\phi = \pi$ (blue) for fixed (c) $T = 338$ fs and (d) $T = 435$ fs using shaped pulse sequence with varying polarization. The photoelectron kinetic energy distribution curves with $T = 338$ fs (red) and $T = 435$ fs (blue) for fixed (e) $\phi = \pi/4$ and (f) $\phi = \pi/2$ using shaped pulse sequence with varying polarization.

To investigate the influence of sub-pulse polarization on the total ionization yield, we compare the above results with the ionization yield using a shaped pulse sequence with constant polarization. The values of parameters A, T, and ϕ are chosen to be the same as those used for the shaped pulse sequence with varying polarization. The two-dimensional ionization yield distribution functions of the phase parameters T and ϕ are shown in Fig. 4. The periodic oscillation of the total ionization yield with T and ϕ still exists, and the oscillation period for T is about 200 fs and for ϕ is 2π. Different from the varying polarization case, the two-dimensional ionization yield pattern is not symmetrical with respect to $\phi = 0$. Two horizontal slices of data from Fig. 4 at $\phi = \pi/2$ and $-\pi/2$ are shown in Fig. 5(a). Again, both yield distributions oscillate with T, and the phase of the oscillation is shifted by π at $\phi = \pi/2$ with respect to that at $\phi = -\pi/2$. The vertical slices of data from the two-dimensional ionization yield distribution in Fig. 4 at $T = 134$ fs and $T = 338$ fs are shown in Fig. 5(b), where the oscillation period is also 2π. Despite some slight differences between Fig. 2 and Fig. 4, the total ionization yield is similarly modulated as functions of T and ϕ using shaped pulse sequences with constant polarization and varying polarization. Therefore the modulation of the total ionization yield seems to be not directly related to the polarization changing of the sub-pulses.

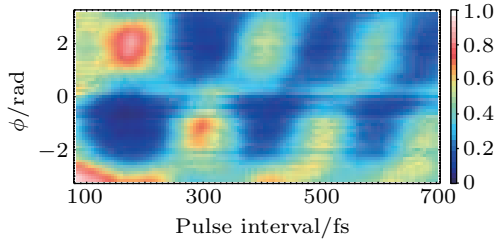


Fig. 4. The ionization yield distribution upon variation of the phase parameters T (pulse interval) from 80 fs to 800 fs and ϕ from $-\pi$ to π for fixed value of $A = 0.5$ using shaped pulse sequence with constant polarization.

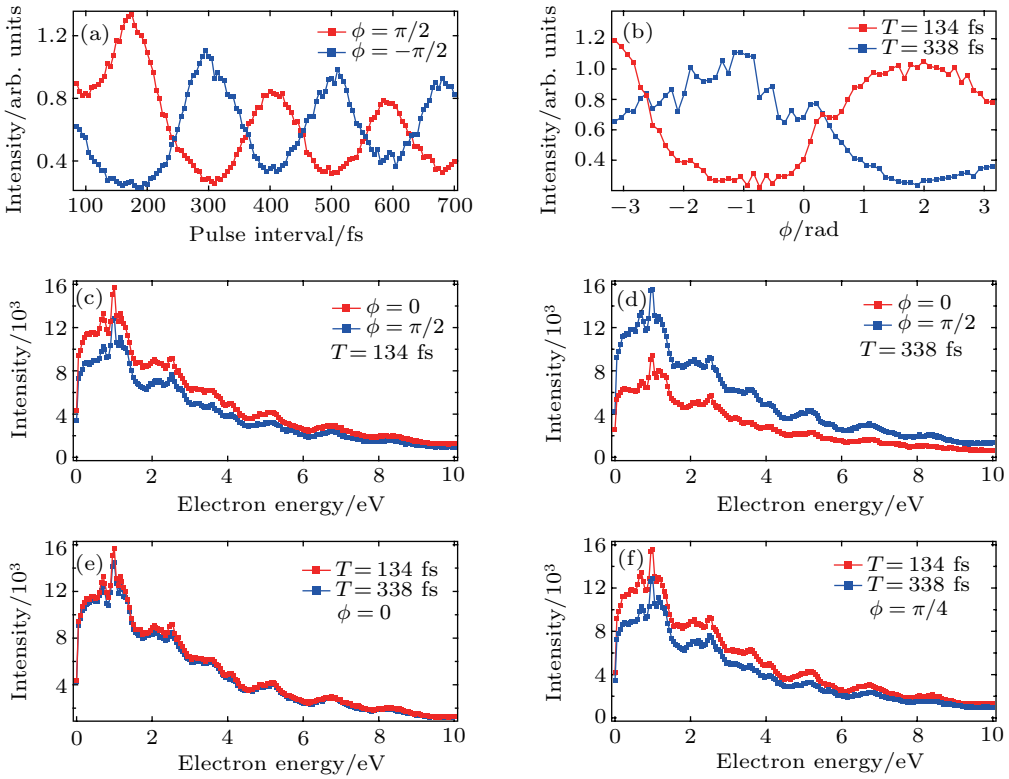


Fig. 5. (a) Horizontal slices of data from the two-dimensional ionization yield distribution in Fig. 4 at $\phi = \pi/2$ (red) and $-\pi/2$ (blue). (b) Vertical slices of data from the two-dimensional ionization yield distribution in Fig. 4 at $T = 134$ fs (red) and $T = 338$ fs (blue). The photoelectron kinetic energy distribution curves with $\phi = 0$ (red) and $\phi = \pi/2$ (blue) for fixed (c) $T = 134$ fs and (d) $T = 338$ fs using shaped pulse sequence with constant polarization. The photoelectron kinetic energy distribution curves with $T = 134$ fs (red) and $T = 338$ fs (blue) for fixed (e) $\phi = 0$ and (f) $\phi = \pi/4$ using a shaped pulse sequence with constant polarization.

To further understand the control mechanism, we first start with a discussion of the ionization mechanism on nitrous oxide irradiated by the shaped pulse. The ionization processes are generally divided into two regimes: multiphoton ionization and tunneling ionization.[30] The Keldysh parameter $\gamma = \sqrt{\frac{I_P}{2U_P}}$, where I_P is the ionization potential, and $U_P = \frac{I}{4\omega^2}$ is the ponderomotive energy (I is the laser intensity, and ω is the angular frequency). The ionization regimes can be identified by the value of γ. When the value of γ is much larger than 1, the ionization process belongs to the multiphoton regime. When the value of γ is close to 1, we generally consider that the ionization process is converted from the multi-

photon regime to the tunneling regime and the potential energy level is modified by the strong coupling of Coulomb and laser field potentials.[31] In our experiment, $I_p = 12.89$ eV, and I is set to about 2×10^{14} W/cm^2. We can obtain $\gamma\approx0.7$, therefore, the tunneling ionization dominates the ionization processes. In addition, the ionization processes undergo predominantly nonresonant excitation under the laser condition, which can be confirmed by the existing energy level information of nitrous oxide[32–35] and the absence of obvious resonance pattern in the measured photoelectron spectrum (photoelectron spectrum data will be presented and discussed in a follow up paper). We also investigate the photoelectron kinetic energy distribution using shaped pulses with both constant polarization and varying polarization. The phase parameters are chosen to be at the point where the coherent control is of the highest efficiency, i.e., the point (or slice) in Fig. 2 where the modulation depth is at maximum. In the experimental results using shaped pulse with varying polarization, we find that the shapes of photoelectron kinetic energy distribution curves with different ϕ and the same T are similar. For example, the curve with $\phi=0$ is very similar to that with $\phi=\pi$ for a fixed $T=338$ fs, as shown in Fig. 3(c), and the curve with $\phi=0$ is also very similar to that with $\phi=\pi$ for a fixed $T=435$ fs, as shown in Fig. 3(d). The shapes of curves with different T and same ϕ are also similar, as shown in Figs. 3(e) and 3(f). The same phenomenon exists in the results using shaped pulses with constant polarization, as shown in Figs. 5(c)–5(f). Thus, the modulation of each ionization channel is similar, and the control on the total ionization yield appears to be the result of combined contribution from all ionization channels rather than the result of enhancing or suppressing of few specific ionization channels.

We find that the same modulation of all ionization processes leads to the control over the total ionization yield, which is different from most strong-field-induced coherent control experiments. As described above, the energy levels of the molecule system will be broadened and shifted under the strong laser irradiation. Therefore, the time-domain structure and phase of pulses become more important. The laser spectral phase is no longer directly related to the interference of the excitation channels. Even though the spectral phase modulation adapts well in weak field regimes, it can only achieve the coherent exciting or switching on few specific quantum channels. In the present experiment, the control of each ionization channel is accomplished by the constructive and destructive interferences of different photons, which has been discussed before[11] and proved to be pulse-bandwidth and spectral phase dependent.[36] Because the laser field has a broad spectrum, it can produce a wide coherent area of ionization pathways. For instance, for a two-photon ionization channel with particular initial-to-final state ($2\omega=(E_i-E_j)/\hbar$),[20] some new pathways are produced between two photons with different frequencies ($\omega_m+\omega_n=(E_i-E_j)/\hbar$) within the bandwidth, which will be discussed in detail later. Previous work has also pointed out that only resonant interference is present in the weak-field limit, but the measured interference changes largely between resonant and nonresonant excitation pathways with the full spectrum and intense pulse.[12] Since the energy levels are dressed and distorted by the strong laser field, we propose that the system is first excited incoherently to the distorted Rydberg state, and then ionizes through coherent nonresonant excitation produced by spectral phase interference of photons. It must be noted that different ionization channels may go through different intermediate Rydberg states distorted by the strong laser field. These incoherent transitions from initial state to intermediate state do not contribute to the control on the total ionization yield, and only the coherent excitations from intermediate state to final state lead to the control on the total ionization yield. Due to the great difference in the probability of multiphoton nonresonant coherent excitation, the probability of two-photon interference is much larger than that of three- and four- photon interference.[37] We study predominantly the two-photon interference of spectral phase. The same discussion has been presented in previous work.[38]

The nonresonant two-photon interference in ionization processes is verified by measuring the second harmonic generation (SHG) signal of the laser field with the same phase parameters using a 0.5-mm-thick BBO crystal. The integrated SHG intensity as functions of the phase parameters T and ϕ is shown in Fig.6. In Fig. 6(a), the spectral intensity integration is done with the full spectral range (396–404 nm) using varying polarization shaped pulse. The pattern of Fig. 6(a) matches poorly with the ionization pattern shown in Fig. 2. However, when the integration range is set to from 399 nm to 401 nm, as shown in Fig. 6(b), the pattern is consistent with the ionization pattern in Fig. 2. Therefore, the two-photon interference causing the control of ionization processes mainly occurs around the laser spectrum center frequency of 400 nm. We believe this is due to the fact that the intensity of the SHG spectrum near the center is larger than that near the side. For the constant polarization case, the pattern in Fig. 6(d) for integration from 399 nm to 401 nm is also more consistent with the ionization pattern in Fig. 4 than that in Fig. 6(c) for integration over the whole range. But the pattern with the integration over the whole range also shows oscillations with T and ϕ, which is not obviously observed in Fig. 6(a) for the varying polarization case. We believe this is due to the influence of the laser pulse structure in the time domain, which needs to be further studied.

The SHG intensity is proportional to the integrated nonlinear power spectrum $I=\int S(\omega)\,\mathrm{d}\omega$,[39] where

$$S(\omega)=\left|\int_{-\infty}^{\infty}E(\omega/2+\Omega)E(\omega/2-\Omega)\,\mathrm{d}\Omega\right|^2 \qquad (10)$$

is the spectral intensity as a function of frequency ω. Here $\omega/2+\Omega$ and $\omega/2-\Omega$ are two of the fundamental frequencies, Ω is the frequency offset, and

$$E(\omega/2+\Omega)=A(\omega/2+\Omega)\exp[\mathrm{i}\varphi(\omega/2+\Omega)] \quad (11)$$

is the Fourier transformation of $E(t)$, where $A(\omega/2+\Omega)$ and $\varphi(\omega/2+\Omega)$ are the spectral amplitude and phase modulated by the shaped phase parameters, respectively. Figures 7(a) and 7(b) show a set of experiment results of the total ionization yield using constant polarization and the theoretical results with two-photon interference model for the same phase parameters, which indicate that our theoretical model generally agrees with the experimental processes. But there are also parts of the curves which do not match well in Fig. 7(a), for instance, at $T<200$ fs. These may be the effects of the shaped pulse structure in time domain, with smaller T, when the step-by-step excitation processes similar to pump–probe processes happen and even the sub-pulses overlap. Although not the main influencing factors, the three-photon and four-photon interference processes should be taken into account for obtaining a perfect match between experimental and theoretical results. In general, we can still prove that the nonresonant two-photon interference processes dominate the control of the total ionization yield.

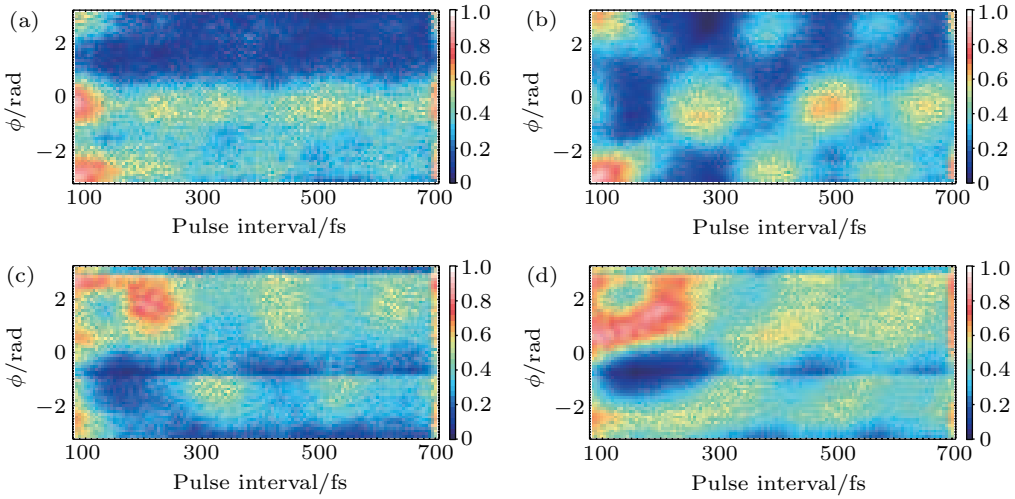


Fig. 6. The integrated SHG intensity as functions of the phase parameters T and ϕ. The spectral intensity integration with the full spectral range (396–404 nm) (a) and from 399 nm to 401 nm (b) using varying polarization shaped pulse. The spectral intensity integration with the full spectral range (396–404 nm) (c) and from 399 nm to 401 nm (d) using constant polarization shaped pulse.

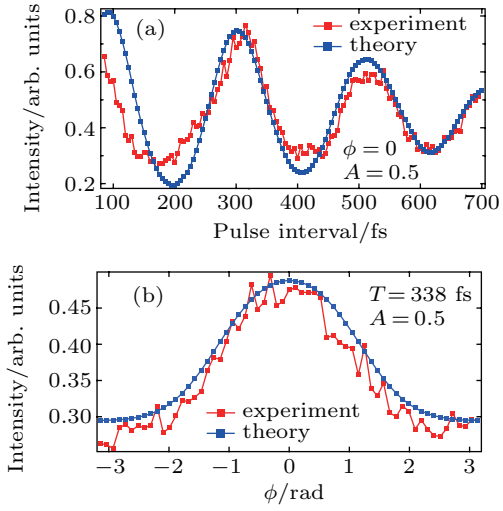


Fig. 7. The measured total ionization yield (red) using constant polarization and the theoretical results with two-photon interference model (blue) for the same phase parameters: (a) varying T with fixed $A=0.5$ and $\phi=0$, (b) varying ϕ with fixed $A=0.5$ and $T=338$ fs.

4. Conclusion

We performed a study of strong-field nonresonant coherent control on ionization using sinusoidal phase modulated laser pulses. The control on the total ionization yield was achieved by the variation of the phase parameters. The influence of laser polarization on ionization processes was discussed using constant polarization and varying polarization shaped pulses. The physical mechanism of control was discussed in detail. Besides the distortion of the energy level in the strong-field, the wide bandwidth of pulse plays a crucial role in the control of ionization processes. The different ionization channels are first excited to the different Rydberg states distorted by the strong laser field, and then experience dominantly the same nonresonant two-photon excitation modulated by the laser phase. The control is accomplished by the constructive and destructive interferences of the nonresonant two-photon excitation. The control mechanism is quite different from previous strong-field coherent control where the time-domain structure and phase of pulse dominate the control. In addition, the ionization is achieved by off-resonant excitation, which indicates that the control is robust, therefore, can likely be expanded to many other applications. The nonresonant two-photon interference in ionization processes was demonstrated experimentally and theoretically by the SHG of

the laser field. However, some experimental phenomena still need to be explained in time domain. For example, the total ionization yield shows obvious attenuation with the increase of T. More likely, strong-field effects, such as multielectron excitation and nonadiabatic effect, also result in the control in our experiment. The present study helps us to better understand the strong-field coherent control, and demonstrates that the physical mechanisms of strong-field coherent control are fairly complicated and further researchable. Further study will focus on the system control in both time and frequency domains. For instance, in the time domain, the wave packets induced by multiple sub-pulses interfere, disperse with the increasing interval of sub-pulse.

References

[1] Shapiro M and Brumer P 1986 *J. Chem. Phys.* **84** 4103
[2] Meshulach D and Silberberg Y 1998 *Nature* **396** 239
[3] Präkelt A, Wollenhaupt M, Sarpe-Tudoran C and Baumert T 1946 *Phys. Rev. A.* **70** 1
[4] Walowicz K A, Pastirk I, Lozovoy V V and Dantus M 2002 *J. Phys. Chem. A* **106** 9369
[5] Ruge M, Wilcken R, Wollenhaupt M, Horn A and Baumert T 2013 *J. Phys. Chem. C* **117** 11780
[6] Dudovich N, Oron D and Silberberg Y 2002 *Phys. Rev. Lett.* **88** 123004
[7] Bayer T, Wollenhaupt M, Sarpe-Tudoran C and Baumert T 2009 *Phys. Rev. Lett.* **102** 023004
[8] Wollenhaupt M, Präkelt A, Sarpe-Tudoran C, Liese D and Baumert T 2006 *Appl. Phys. B* **82** 183
[9] Wollenhaupt M, Präkelt A, Sarpe-Tudoran C, Liese D and Baumert T 2005 *J. Opt. B* **7** S270
[10] Wollenhaupt M, Assion A, Bazhan O, Horn C, Liese D, Sarpe-Tudoran C, Winter M and Baumert T 2003 *Phys. Rev. A* **68** 015401(R)
[11] Gandman A, Chuntonov L, Rybak L and Amitay Z 2007 *Phys. Rev. A* **76** 053419
[12] Clow S and Weinacht T 2010 *Phys. Rev. A* **82** 023411
[13] Hosseini S A and Goswami D 2001 *Phys. Rev. A* **64** 033410
[14] Dudovich N, Oron D and Silberberg Y 2004 *Phys. Rev. Lett.* **92** 103003
[15] Chelkowski S, Bandrauk A D and Corkum P B 2017 *Phys. Rev. A* **95** 053402
[16] Lucchese R R, Lafosse A, Brenot J C, Guyon P M, Houver J C, Lebech M, Raseev G and Dowek D 2002 *Phys. Rev. A* **65** 020702
[17] Marceau C, Makhija V, Platzer D, Naumov A Y, Corkum P B, Stolow A, Villeneuve D M and Hockett P 2017 *Phys. Rev. Lett.* **119** 083401
[18] Tang Y, Suzuki Y I, Horio T and Suzuki T 2010 *Phys. Rev. Lett.* **104** 073002
[19] Suzuki Y I, Tang Y and Suzuki T 2012 *Phys. Chem. Chem. Phys.* **14** 7309
[20] Roslund J and Rabitz H 2014 *Phys. Rev. Lett.* **112** 143001
[21] Pengel D, Kerbstadt S, Johannmeyer D, Englert L, Bayer T and Wollenhaupt M 2017 *Phys. Rev. Lett.* **118** 053003
[22] Lux C, Senftleben A, Sarpe C, Wollenhaupt M and Baumert T 2016 *J. Phys. B: At. Mol. Opt. Phys.* **49** 02LT01
[23] Chen Z, Tong Q N, Zhang C C and Hu Z 2015 *Chin. Phys. B* **24** 043303
[24] Diels J C and Rudolph W 2006 *Ultrashort Laser Pulse Phenomena* (Second edition) (San Diego: Academic Press) p. 452
[25] Wollenhaupt M, Präkelt A, Sarpe-Tudoran C, Liese D, Bayer T and Baumert T 2006 *Phys. Rev. A* **73** 063409
[26] Brixner T and Gerber G 2001 *Opt. Lett.* **26** 557
[27] Li X K, Wang C C, Yuan Z Q, Te D F, Ma P, Hu W H, Kyi S Z, Fu L B and Ding D J 2017 *Phys. Rev. A* **96** 033416
[28] Brixner T, Krampert G, Niklaus P and Gerber G 2002 *Appl. Phys. B* **74** S133
[29] Blanchet V, Nicole C, Bouchene M A and Girard B 1997 *Phys. Rev. Lett.* **78** 2716
[30] Keldysh L V 1965 *Sov. Phys. JETP* **20** 1307
[31] Ivanov M Y, Spanner M and Smirnova O 2005 *J. Mod. Opt.* **52** 165
[32] Bhatt P, Singh R, Yadav N and Shanker R 2012 *Phys. Rev. A* **85** 034702
[33] Moradm, A, Landers A L and Fogle M 2013 *Phys. Rev. A* **88** 012713
[34] Chen W and Liu J 2003 *J. Phys. Chem. A* **107** 8086
[35] Kostko O, Kim S K, Leone S R and Ahmed M 2009 *J. Phys. Chem. A* **113** 14206
[36] Carroll E C, Pearson B J, Florean A C, Bucksbaum P H and Sension R J 2006 *J. Chem. Phys.* **124** 114506
[37] Lozovoy V V and Dantus M 2005 *Chem. Phys. Chem.* **6** 1970
[38] Dudovich N, Polack T, Pe'er A and Silberberg Y 2005 *Phys. Rev. Lett.* **94** 083002
[39] Meshulach D and Silberberg Y 1999 *Phys. Rev. A* **60** 1287